Study on the evacuation of gas in bulk-fill insulation materials used in large-scale LH2 storage tanks

Clara Mata, Rob Hunter, Andrew Peterson , Matt Mortensen

Abstract

Large-scale hydrogen storage is crucial for advancing liquid hydrogen technology. Due to liquid hydrogen's ultra-low boiling point and low heat of vaporization, effective insulation is necessary to minimize boil-off loss. Larger storage vessels use bulk-fill insulation like perlite and hollow glass microspheres (glass bubbles) operating at moderate vacuum (MV) levels. The choice of insulation material affects the construction schedule, capital cost, and operating costs of storage tanks. Therefore, studying evacuation properties of bulk-fill insulation materials is essential to advance hydrogen-based energy infrastructure. This study aimed to quantify and compare the pump-down times for 3M™ Glass Bubbles K1 and cryo-insulation grade perlite and to identify physical properties influencing pump-down times. Perlite, with its porous structure and low bulk density, was expected to enable faster gas evacuation, while glass bubbles were thought to hinder it. However, our research shows that dry 3M™ Glass Bubbles K1 have faster nitrogen evacuation rates.

1. Introduction

Renewable energy production varies by region. To achieve carbon neutrality goals, countries lacking renewable resources can consider importing them from countries with abundant renewables [1–8]. Hydrogen, with its high energy density, is recognized as a versatile energy carrier and efficient storage medium for achieving a decarbonized global energy system [9–20].

To successfully advance liquid hydrogen (LH2) technology and its application in different sectors, the establishment of large-scale hydrogen storage (ranging from 20,000 to 100,000 m3) is crucial [21–25]. This storage capacity plays a vital role in the global hydrogen supply chain, serving not only onshore storage needs but also offshore storage, particularly for shipping and maritime applications [26,27].

Ensuring the widespread commercial use and feasibility of hydrogen technology requires the development of cost-effective and safe storage and transportation technologies for LH2 [9,13,21,28,29,30]. These technologies are essential for both stationary applications and offshore transportation [26,31]. Due to liquid hydrogen's ultra-low boiling point (20 K) and low heat of vaporization, effective insulation is necessary for storage tanks to minimize boil-off loss [13,31,32,33,34]. Additionally, proper safety measures must be implemented to handle the vent gas [35], as hydrogen has a wide flammability range when mixed with air [26].

Insulation systems play a crucial role in ensuring the performance of liquid hydrogen storage tanks [31,34,36]. Smaller tanks with capacities ranging from 100 to 1000 m3 typically utilize high-vacuum (HV) multi-layer insulation (MLI), while larger storage vessels employ bulk fill insulation operating at moderate vacuum (MV) levels [37]. Commonly used bulk fill insulation materials include perlite and hollow glass microspheres (glass bubbles) [31,38,39]. However, according to conventional wisdom the choice of insulation material affects the construction schedule, capital cost, and operating costs of storage tanks through heat leak and long-term maintenance [31].

Hollow glass microspheres offer a cryogenic insulation system that is lightweight, durable, and requires minimal maintenance [40]. 3M™ Glass Bubbles K1 outperform perlite by reducing stored LH2 (liquid hydrogen) boil-off by 46% in evacuated cryo-insulation [41]. In fact, “glass bubbles are superior to perlite powder across the entire pressure range.” This improved performance is primarily attributed to the additional radiation scattering provided by the walls of the glass bubbles, along with the low thermal conduction resulting from the point contacts between adjacent spheres [42]. These factors contribute to better insulation properties and reduced heat transfer, resulting in lower LH2 boil-off rates

However, while thermal performance advantages are significant, they come with associated material and construction costs [31]. For example, a recent study in the literature highlights a 2x to 4x increase in the time required to achieve the desired vacuum in the insulation annulus for a vessel filled with glass bubbles compared to one filled with perlite [37].

Table 1
Tank dimensions used to model the thermal performance of a 5000 m3 tank

Dimensions	Tank 1	Tank 2
Capacity, m^3	218	5000
Outer Diameter, m	9.3	24.6
Insulation layer thickness, m	1	1.7

Table 2
Impact of 1-year of liquid hydrogen boil-off reduction in a 5000m^3 tank when glass bubbles are used as cryogenic insulation instead of perlite.

	Seawater Reverse Osmosis	900-Watt A/C unit	American Household	Cooling of 1 Average Data Center
Energy Requirement	4 kWh/m^3	7.2 kWh/8-h	10,500 kWh/household/year	575 MWh/day
Result of using 742 MWh 1 day				1.3 data centers cooled
Result of using 742 MWh 1 year	185,609 m^3	103,116 8-h periods of cooling	70.7 households powered	

the time required to achieve the desired vacuum in the insulation annulus for a vessel filled with glass bubbles compared to one filled with perlite [37].

The question is whether the apparent increase in construction time can be seen as a long-term investment and commitment to a decarbonized and sustainable world. For instance, what would be the impact of saving 1 year of hydrogen loss due to boil-off if glass bubbles were used to insulate a 5000 m3 LH2 storage tank?

To answer this question, we modeled the thermal performance of a 5000 m^3 tank, similar in size to the world's largest LH2 storage tank located in Florida, USA [43,44]. Reported LH2 boil-off rate values for glass bubbles and perlite for a smaller tank [45] were adjusted for the target size of 5000 m^3 using the Fourier's Law of thermal conduction [46]. This analysis focused on heat leak through the insulation material layer only, neglecting the tank wall thickness. Key factors, such as structural heat loads (i.e. heat leak through supports, piping, etc.) were assumed to be constant between the two tanks, denoted by the subscripts 1 and 2. Briefly,

$$\frac{NER_1}{NER_2} \approx \left(\frac{\Delta R_2}{\Delta R_1}\right) \frac{\left(A_{wetted}/V_{wetted}\right)_1}{\left(A_{wetted}/V_{wetted}\right)_2},$$

where *NER* is the ratio of the normal evaporation rate (percentage of the total liquid volume/mass that boils-off as a result of heat leak), ΔR is the insulation layer thickness, and A_{wetted}/V_{wetted} is the wetted surface areato-volume ratio. Equation (1) implies constant insulation material effective thermal conductivity ke and, heat of vaporization of the liquid hydrogen h_{fg}.

Values in the right-hand side of Equation (1) were calculated using the tank dimensions listed in Table 1. The insulation thickness for Tank 2 matches the thickness of the world largest LH2 storage tank with a capacity of 4700 m^3, with inner and outer diameters of 21.9 m and 25.3 m, respectively [44]. An ullage of 10% was assumed to determine A_{wetted}/V_{wetted}.

Six years of testing of a 218 m3 spherical tank insulated with glass bubbles yielded an average NER of 0.10% per day, or 208 l/day, resulting in 46% boil-off reduction when compared to 0.18% per day (386 l/day), the perlite baseline boil-off for the same time [41].

Calculated NER values for Tank 2 per equation (1) are 0.02% per day (1033 l/day) for glass bubbles, and 0.04% per day (1918 l/day) for perlite. The use of glass bubbles instead of perlite for one year would result in more than 322,000 l of liquid hydrogen saved from boil-off (884 l/day reduction), or 742 MWh in energy saved considering liquid hydrogen has a volumetric energy density of 2.3 kWh/l [47].

742 MWh of energy in one year can be utilized in various ways. For instance, it can be used to purify approximately 185,609 m3 of seawater through reverse osmosis [48–50]. The same amount of energy can provide cooling for approximately 130,116 8-h periods using a 900-Watt air conditioner. Furthermore, it has the potential to power 70.7 American households for an entire year [51]. Lastly, it can provide cooling for an average data center for approximately 1.3 days [52,53] (Table 2). These numbers hold great significance, especially when considering the global warming crisis and its impact on health [54–56].

Nonetheless, efforts to minimize construction time should be prioritized. Rigorous characterization of different bulk-fill materials can help to identify "clear and standardized work procedures for material injection and vacuum formation that can greatly reduce the construction period of LH2 storage tanks" [57].

Bulk-fill insulation materials have varying properties that can impact the efficiency of the evacuation process [31]. By studying and comparing these properties, cryogenic storage tank designers and researchers can make informed decisions regarding the selection of bulk-fill insulation materials, ultimately leading to improved evacuation

rates and enhanced overall system performance. This knowledge is essential for the development and optimization of efficient and reliable hydrogen-based energy systems.

Our primary objectives were twofold: (1) Quantify and compare the pump-down times for 3M™ Glass Bubbles K1 and cryo-insulation grade perlite; and (2) Identify the physical properties and other parameters that may influence the pump-down times. By focusing on these aspects, we aimed to shed light on the factors that contribute to the observed variations in evacuation times between the two bulk-fill insulation materials. In the subsequent sections, we will outline the experimental methodology, present the results of our investigation, and discuss the implications of our findings.

2. Materials and methods

2.1. Experimental setup

To create a variable vacuum environment ranging from ambient to 10 mTorr (1.33 Pa), a rotary vacuum pump (Edwards, model E2M40) was fitted to a 10L stainless-steel cylinder (Fig. 1).

The cylinder was equipped with a sintered HDPE porous tube (POREX™) and a high vacuum puppet valve (ANCORP, AV150-QF-EAS). During the evacuation process, the pressure was measured using a pressure transducer (Grandville-Phillips, 275 Convectron, catalog 275071).

The pressure transducer was positioned between the pump and the cylinder, and its readings were monitored by laboratory personnel throughout the entire desired range. This allowed for accurate measurement and tracking of the evacuation process.

The stainless-steel cylinder can be heated with a heating belt partially insulated by an external insulation grey jacket. The temperature is controlled using two rheostats (not shown) connected to thermocouples located on the external wall of the cylinder

Other equipment includes an analytical balance (Mettler-Toledo, XPE64001L), a gas pycnometer (Micromeritics, Accupyc II 1345) and a Particle Size Distribution (PSD) Analyzer (Microtrac, S3500 in water, in air).

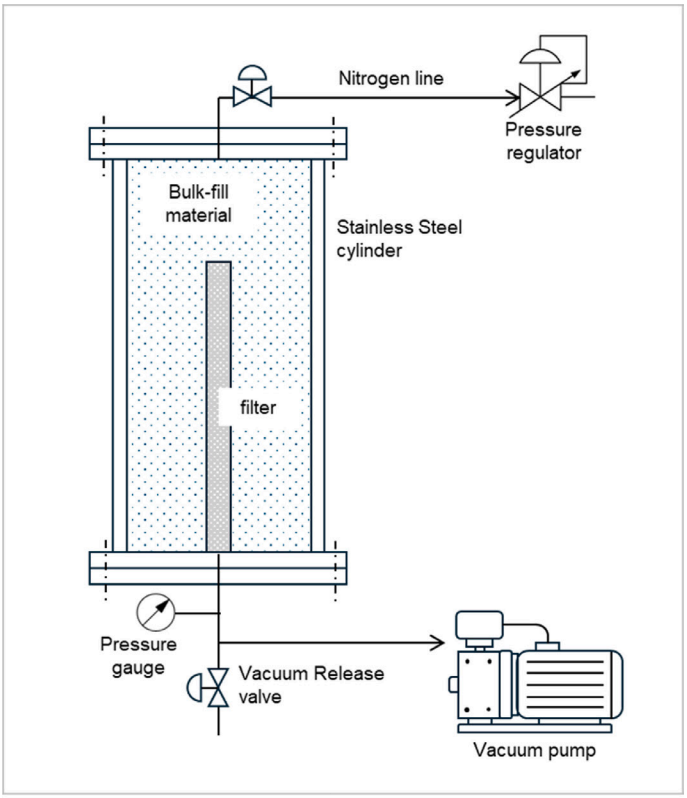

(a)

(b)

Fig. 1. Experimental Set Up. (a) Schematic illustrating the gas evacuation path and position of a single pressure gauge; and (b) Photograph of stainless-steel cylinder interior where the filter (sintered HDPE porous tube) can be seen.

2.2. Procedure

The insulating material is carefully poured from a pre-weighed bag into the stainless-steel cylinder. The material is gently compacted by periodically pulling a vacuum every few minutes until the cylinder is completely filled. To determine the total powder mass in the cylinder, the bag is re-weighed, and the net mass is calculated by taking the difference.

Once the cylinder is filled and sealed, the initial conditions inside the chamber, such as internal pressure and exterior wall temperature, are recorded. Additionally, the room conditions (temperature and relative humidity) are logged for reference. The vacuum pump is then started, and the air inside the chamber is gradually evacuated until a minimum pressure of 10 mTorr (1.33 Pa) is achieved. Pressure as a function of time (monitored using a digital timer), is manually logged.

Once the desired vacuum pressure of 10 mTorr (1.33 Pa) has been achieved the system can be re-pressurized back to ambient pressure by venting it with nitrogen, and a second pump-down test can be run as described earlier.

In addition to hollow glass microspheres and cryo-insulation grade perlite, other particles evaluated in this study include glass marbles (16 mm dia.) and ceramic spheres (390 µm dia.)

2.3. Insulating materials characterization

Hollow glass microspheres, specifically 3M™ Glass Bubbles K1, and cryo-insulation grade perlite obtained from three different sources (A, B and C) were subjected to thorough characterization in this study.

Table 3 presents the typical average true density, bulk density, and volatiles (assumed to be entirely water) of the bulk-fill insulation materials under study. These properties are essential for understanding the overall density and moisture content of the materials, which can impact their insulation performance.

Table 3
Typical average properties of 3M™ Glass Bubbles K1 and cryo-insulation grade perlite.

Typical Physical Property	3M™ Glass Bubbles K1	Cryo-insulation grade perlite
Isostatic Crush Strength (80% survival)	250 psi (1.72 MPa)	
True density (gas pycnometry)	125 kg/m^3	
Bulk density (closed packed)	78 kg/m^3	88 kg/m^3
Volatile content (water)	0.3 wt%	0.6 wt%
Mean Size[a]	56 µm	671 µm

[a] *measured.*

Additionally, Table 4 provides a comprehensive summary of the measured particle size distributions (PSD) of the materials, as depicted in Fig. 2. Analyzing the particle size distributions is crucial for assessing the size range and distribution of the particles, which can influence their thermal and mechanical properties as cryogenic insulation materials.

Table 4
Measured Particle Size Distribution (µm) of 3M™ Glass Bubbles K1 and cryo-insulation grade perlite by volume.

Product	3M™ Glass Bubbles K1	Cryo-insulation grade perlite
Mean	56	671
Median	55	607
Mode	66	751
SD	24	451
<5th%	19	92
<10th%	25	98
<50th%	55	607
<90th%	89	1322
<95th%	134	1550

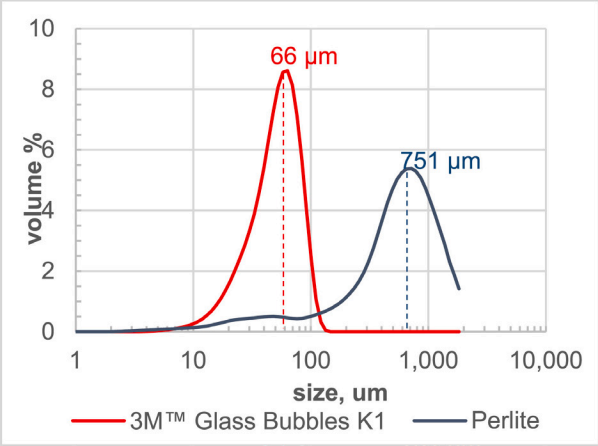

Fig. 2. Measured Particle Size Distribution of 3M™ Glass Bubbles K1 and cryo-insulation grade perlite.

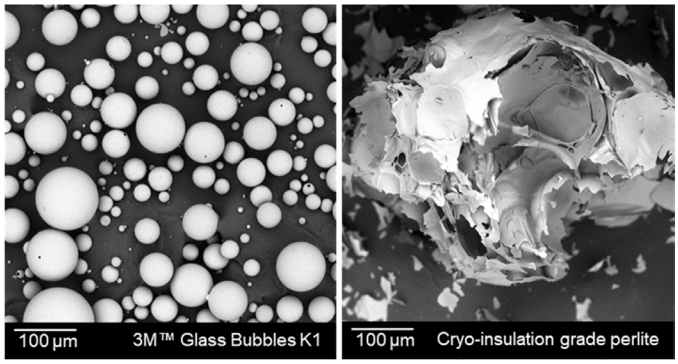

Fig. 3. Scanning Electron Micrographs (SEM) of materials used in the study: 3M™ Glass Bubbles K1 (left) and cryo-insulation grade perlite (right).

In addition to size, particle size distribution (PSD), and surface area, other physical properties of bulk-fill insulation materials may have an impact on pump-down times. To further investigate these properties, additional material characterization tests were conducted using a universal powder rheometer (Micromeritics, FT4). The additional tests include permeability, shear cell, and flowability tests.

Permeability testing assesses how well gases or fluids can pass through a powder bed. Shear cell tests measure the shear stress at the point where the powder starts to flow [58]. Flowability testing evaluates how easily materials can flow under specific conditions. By conducting these comprehensive powder-rheology tests, a deeper understanding of the physical properties of the bulk-fill insulation materials and their potential impact on pump-down times can be gained.

2.3.1 FT4 permeability tests

Fig. 4 depicts plots of nitrogen flux as a function of pressure drop for pre-consolidated 3M™ Glass Bubbles K1 and cryo-insulation grade Perlite B. The data was obtained per ASTM D6539-13. Linear regressions we used to calculate permeability values according to Darcy's Law (Table 5).

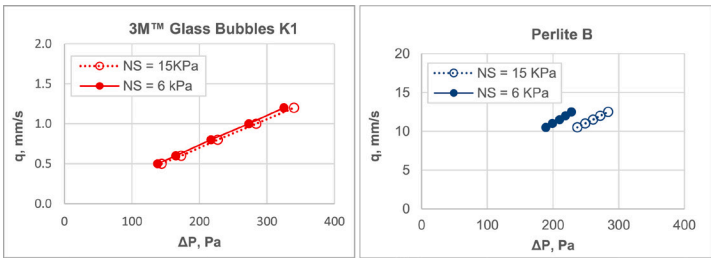

Fig. 4. Nitrogen flux vs pressure drop for pre-consolidated 3M™ Glass Bubbles K1 (left), and cryo-insulation grade Perlite B (right). Pre-consolidating Normal Stresses (NS) include 6 and 15 kPa.

Table 5
Measured permeability at different pre-consolidating normal stresses for 3M™ Glass Bubbles K1 and cryo-insulation grade perlite.

Product	3M™ Glass Bubbles K1	Perlite B
True Density (Kg/m^3)	125	725
k @ 6 kPa (Darcy)	2.53	32.6
k @ 9 kPa (Darcy)	2.45	29.1
k @ 15 kPa (Darcy)	2.35	24.2

Compared to *Perlite B*, 3M™ Glass Bubbles K1 are less sensitive to the pre-consolidating normal stresses. They also show permeability k values 10x smaller, which could possibly impact pump-down times.

2.3.2. FT4 standard shear cell test

The flow initiation properties of 3M™ Glass Bubbles K1 and cryo-insulation grade *Perlite A, B* and *C* were evaluated using the ASTM D7891–15 standard. Fig. 5 depicts curves of incipient shear stress as a function of applied normal stress for various pre-consolidating normal stresses. It is evident from the graph that K1 glass bubbles show lower sensitivity to the pre-consolidating normal stress when compared to cryo-insulation grade *Perlite B*.

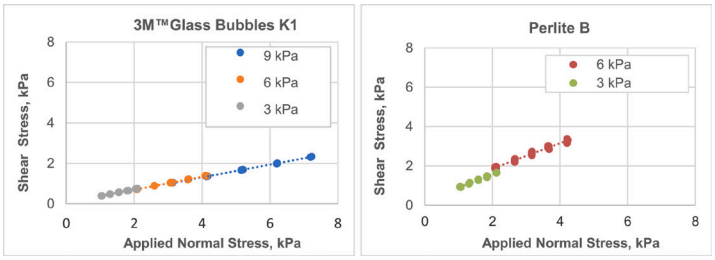

Fig. 5. Incipient Shear Stress vs. Applied Normal Stress (NS) for 3M™ Glass Bubbles K1 (left), and cryo-insulation grade Perlite B (right).

Fig. 6 displays curves of Incipient Shear Stress vs. Applied Normal Stress for 3M™ Glass Bubbles K1 and *Perlite A, B*, and *C*, all under a pre-consolidating normal stress of 6 KPa. Mohr's circle principles were applied to calculate shear parameters that are commonly employed in the design of storage hoppers and bins, following industry-standard calculation procedures. Only two of these parameters are reported in Table 6: *Cohesion* (y-axis intercept) and *Angle of Internal Friction* (slope).

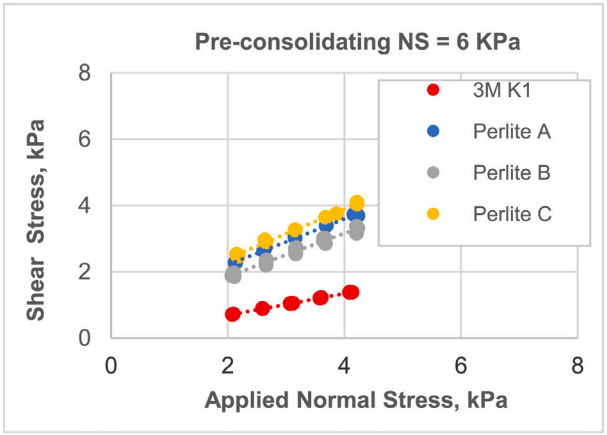

Fig. 6. Incipient Shear Stress vs. Applied Normal Stress for 3M™ Glass Bubbles K1 and cryo-insulation grade perlites.

Table 6
Cohesion and *Angle of Internal Friction* for 3M™ Glass Bubbles K1, and cryo-insulation grade perlites.

Product	Cohesion (kPa)	AIF (°)
3M™ Glass Bubbles K1	0.0341	18.1
Perlite A	0.829	34.6
Perlite B	0.569	32.9
Perlite C	0.908	36.7

In comparison to *Perlite A*, *B*, and *C*, 3M™ Glass Bubbles K1 exhibit lower *Cohesion* by one order of magnitude. Additionally, they have an *Angle of Internal Friction* that is half of that observed in the perlite samples.

The bulk-fill insulation material's cohesion and other shear properties can potentially influence the pump-down time. For instance, it could have an effect on the packing factor of the material as it is being placed (by gravity) in the annulus of a cryogenics vessel. More cohesion could result in less efficient packing, impacting permeability.

2.3.3. FT4 basic flow test

Flowability is not an inherent property of powder but rather a function of its ability to flow as required in a specific application [59]. In fact, powder flowability significantly impacts transportation, mixing, and processing, thereby affecting manufacturing, storage, and application efficiency [60]. For instance, when aerated, glass bubbles flow like a liquid, facilitating the complete filling of annular spaces and conforming to complex geometries formed by structural supports and piping. Preventing insulation voids is crucial, as they affect the thermal performance of the vessel insulation system [37].

3M™ Glass Bubbles K1 and cryo-insulation grade Perlite B were characterized in terms of *Basic Flowability Energy* (BFE), *Stability Index* (SI), *Flow Rate Index* (FRI), *Specific Energy* (SE), and *Conditioned Bulk Density* (CBD), by applying "a unique *Dynamic Methodology* for measuring the resistance of a powder to flow, while the powder is in motion" [61].

Although bulk properties are not a direct measurement of flowability, they can influence process performance and product attributes. To remove any stress history or excess air prior to testing, an automatic conditioned step is completed before every flow test. Gentle displacement of the whole sample loosens and slightly aerates the powder conditioning it to produce a homogeneously packed powder bed. Conditioning also reduces operator-to-operator variability and ensures reproducibility [61].

Flowability test results are summarized in Table 7. Compared to *Perlite B*, 3M™ Glass Bubbles K1 require less than half the energy to be displaced during downward testing (BFE) and require less energy per gram to be displaced during upward testing (SE); all of this in spite of packing more efficiently (CBD).

Table 7
Basic Flow Energy and other parameters.

Product	BFE (mJ)	SI	FRI	SE (mJ/g)	CBD (Kg/m³)
3M™ Glass Bubbles K1	37.6	1.04	1.45	3.00	68
Perlite B	82.9	0.90	1.32	4.95	45

Values of SI (factor by which the measured flow energy changes during repeated testing or processing) show that 3M™ Glass Bubbles K1 are slightly more stable than Perlite B. In the other hand, values of FRI (factor by which the measured flow energy is changed when the flow rate is reduced by a factor of 10) suggest that K1 glass bubbles more sensitive to changes in flow rate.

3. Results and discussion

The evacuation properties of a stainless-steel cylinder filled with 3M™ Glass Bubbles K1 and cryo-insulation perlite were studied to assess the rates of evacuation and identify the factors that influence these rates.

3.1. Vacuum formation for "as is" 3M™ Glass Bubbles K1 and "as is" (packaged) cryo-insulation grade perlite

Fig. 7 illustrates the pressure versus time curves for both bulk-fill insulation materials as air is evacuated from the stainless-steel cylinder at room temperature (RT). The evacuation process down to 100 mTorr (13.33 Pa) is comparable for both materials. However, beyond that point, a noticeable decrease in the rate of vacuum formation is observed for the 3M™ Glass Bubbles K1.

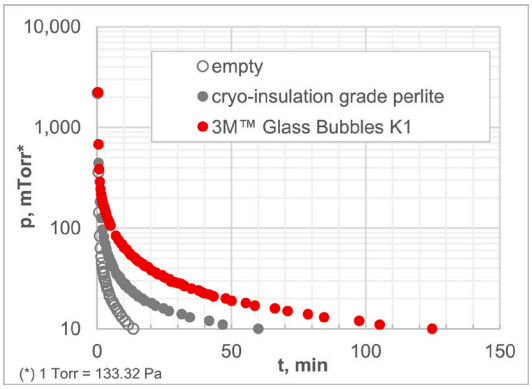

Fig. 7. Plot of pressure vs. time as air is evacuated at room temperature.

In comparison to cryo-insulation grade perlite, it takes twice as long to reach 10 mTorr (1.33 Pa) when evacuating the chamber filled with 3M™ Glass Bubbles K1(Table 8). This finding aligns with the generalized estimates for vacuum pump-down recently reported by Swanger et al. [37].

Table 8
Pump-down time when air is evacuated at RT (stage 1), followed by re-pressurizing of the system with nitrogen, and nitrogen evacuation at RT (stage 2).

Evacuated gas	**air (stage 1)**		
Material	Moisture Level	Time to 100 mTorr[a]	Time to 10 mTorr
3M™ Glass Bubbles K1	As received	5 min	125 min
Cryo-insulation grade perlite	As received	2 min	60 min

[a] 1 Torr = 133.32 Pa.

Evacuated gas	**air (stage 2)**		
Material	Moisture Level	Time to 100 mTorr[a]	Time to 10 mTorr
3M™ Glass Bubbles K1	Vacuum dried at RT		90 s
Cryo-insulation grade perlite	Vacuum dried at RT	42 s	146 s

Following the evacuation of air at room temperature (RT) and subsequent re-pressurization to ambient pressure with nitrogen, the glass bubble-filled cylinder exhibits a notably faster vacuum formation rate compared to the perlite-filled cylinder, as illustrated in Fig. 8. This finding suggests that the presence of moisture in the bulk-fill insulation materials could have a substantial effect on the pump-down times. Once the moisture is eliminated, other factors are likely to come into play and influence the rate at which the vacuum is formed.

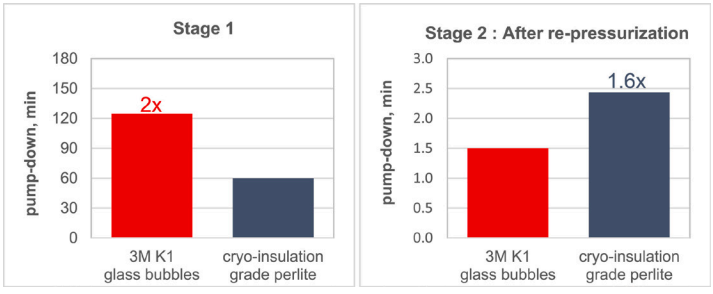

Fig. 8. Pump-down time to 10 mTorr (1.33 Pa) when air is evacuated (Stage 1), followed by re-pressurizing of the system with nitrogen, and nitrogen evacuation (Stage 2).

3.2. Effect of moisture on 3M™ Glass Bubbles K1

Fig. 9 presents the pressure versus time curves for K1 glass bubbles under two conditions: "as is" and conditioned (subjected to 40 °C/90%rh for 3 days). The graph reveals that the evacuation process down to 30 mTorr (4.0 Pa) remains largely unaffected by the moisture level. However, beyond this threshold, a distinct decrease in the rate of vacuum formation becomes evident, suggesting significant impact of moisture on the process.

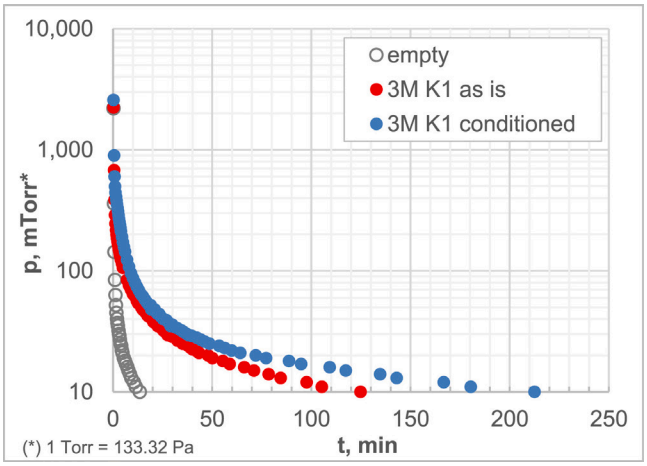

Fig. 9. Plot of pressure vs time as air is evacuated from the stainless-steel cylinder filled with 3M™ K1 Glass Bubbles under two conditions: "as is" and conditioned (subjected 40 °C/90%rh for 3 days).

The pump-down time increases by 70% when air is evacuated from cylinder filled with conditioned glass bubbles compared to "as is" glass bubbles (Fig. 10). This indicates that moisture management should be taken into consideration when optimizing pump-down times. Managing moisture effectively can help reduce the pump-down time and improve the overall efficiency of the process.

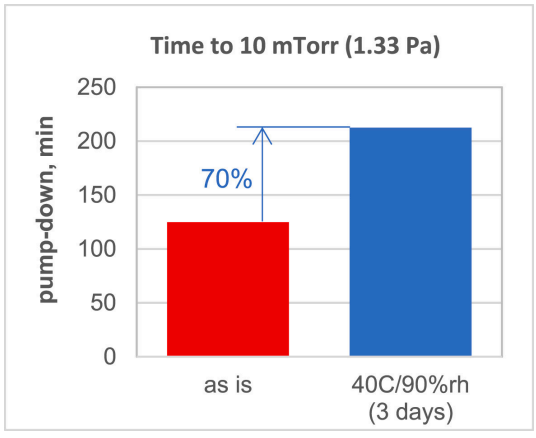

Fig. 10. Pump-down time to 10 mTorr (1.33 Pa) when air is evacuated from the stainless-steel cylinder filled with 3M™ Glass Bubbles K1 under two conditions: "as is" and conditioned (subjected 40 °C/90%rh for 3 days).

3.3. Effect of particle size/surface area (while maintaining packing efficiency constant)

While the random packing density of mono-sized spheres is about 0.64 [62], the reported average packing factor of 3M™ Glass Bubbles K1 averages about 60% [63].

Pressure vs. time curves for various smooth surface spherical particles, including 3M™ Glass Bubbles K1 are shown in Fig. 11. Since these particles have a spherical shape and a narrow and/or monomodal particle size distribution, it is expected that they will occupy roughly 60% of the stainless-steel cylinder. This means that the total volume of gas to be evacuated is roughly the same for all these particles. In this case, the remaining independent parameter is the average particle size, which directly affects the surface area. As the average particle size decreases, the surface area increases. In fact, the surface area is inversely proportional to the square of the particle size.

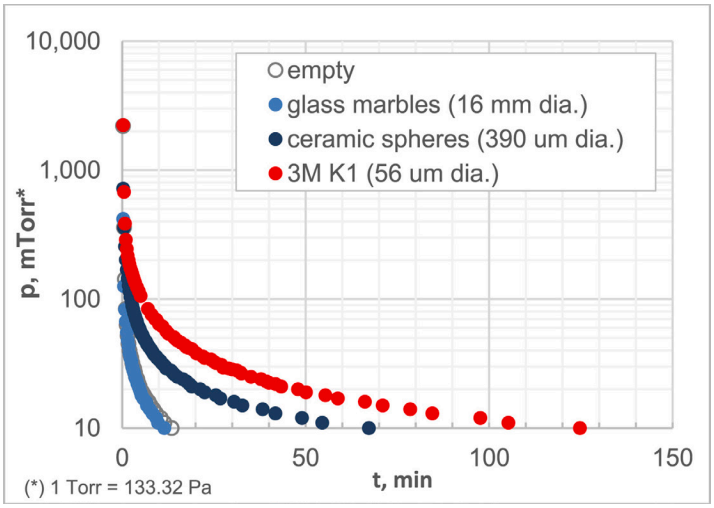

Fig. 11. Plot of pressure vs time for smooth surface, spherical particles as air is evacuated at room temperature.

As depicted, the smaller the particle size the longer it takes to evacuate the system (Fig. 11); suggesting that surface area affects the pump-down time.

As more surface area is available, more moisture can adsorb to the particles per unit volume, increasing the total amount of moisture to be evacuated, as thus the air pump-down time (Table 9).

Table 9
Average evacuation time for smooth spherical particles of different sizes, when air is evacuated at RT (stage 1), followed by re-pressurizing of the system with nitrogen, and nitrogen evacuation at RT (stage 2).

Evacuated gas	**air (stage 1)**			
Material	Average Diameter	Moisture Level	Time to 100 mTorr[a]	Time to 10 mTorr
empty		As is	1 min	14 min
Glass marbles	16 mm	As received	1 min	12 min
Ceramic spheres	0.39 mm	As received	2 min	67 min
3M™ Glass Bubbles K1	56 µm	As received	5 min	125 min

[a] 1 Torr = 133.32 Pa.

Evacuated gas	**nitrogen (stage 2)**			
Material	Average Diameter	Moisture Level	Time to 100 mTorr[a]	Time to 10 mTorr
empty		Vacuum dried at RT	47 s	103 s
Glass marbles	16 mm	Vacuum dried at RT	32 s	47 s
Ceramic spheres	0.39 mm	Vacuum dried at RT	23 s	67 s
3M™ Glass Bubbles K1	56 µm	Vacuum dried at RT		90 s

Once air + moisture has been evacuated at RT and the cylinder is re-pressurized with nitrogen, pump-down times are significantly reduced (Fig. 12).

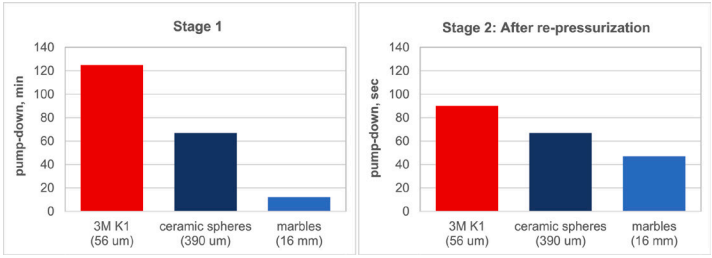

Fig. 12. Pump-down time to 10 mTorr (1.33 Pa) when air is evacuated (Stage 1), followed by re-pressurizing of the chamber with nitrogen, and nitrogen evacuation (Stage 2).

Although evacuating air down to 10 mTorr (1.33 Pa) at RT removes a considerable portion of the present moisture, resulting in significantly shorter nitrogen evacuation times (compared to air), residual moisture (proportional to surface area) may have minor but noticeable effect on nitrogen pump-down times.

Other parameters associated with particle size, PSD and surface area that can potentially impact pump-down times are the permeability k of the particle system (effect on gas free path) and particle surface roughness (effect on moisture-surface bond).

3.4. Effect of temperature

In large scale field applications perlite is expanded in-situ, which minimizes moisture adsorption as the perlite is dispensed into the insulation section of double wall cryogenic vessels.

In an attempt to remove as much moisture as possible from the "as is" (packaged) perlite, heat was applied to the stainless-steel cylinder filled with perlite until a temperature of 90 °C of the exterior wall of the cylinder was achieved. Only then, the vacuum pump was started.

Fig. 13 shows pressure vs. time curves for packaged perlite for two different temperatures. The 'pre-heated' perlite (90 °C) showed a significantly longer evacuation time compared to the 'as is' (RT) perlite. A possible explanation is that considerably more moisture became available, increasing the pump-down time by 10-fold.

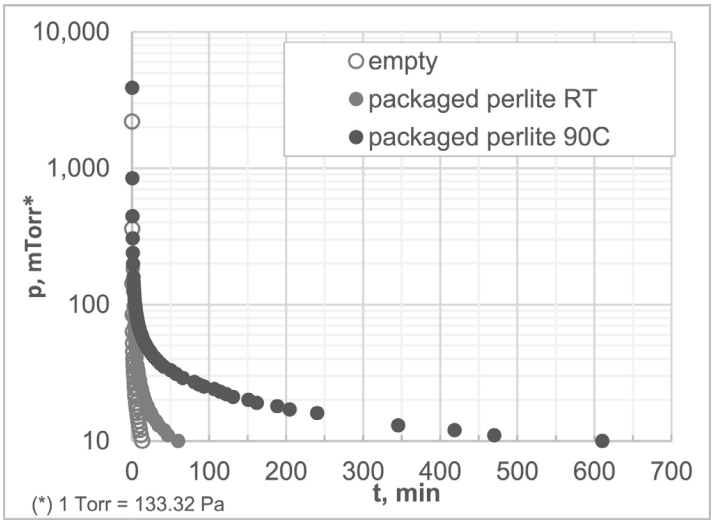

Fig. 13. Plot of pressure versus time for packaged perlite as air is evacuated from the stainless-steel cylinder at RT and 90 °C.

We also believe that more residual moisture remained trapped not only on the rough exterior surfaces of the perlite particles, but also inside the internal multi-cellular spaces (Fig. 2). This would explain why it took longer to evacuate nitrogen after the perlite had been vacuum dried at 90 °C (Table 10).

Table 10
Average Evacuation time for packaged perlite, first air (at RT and 90 °C) and then nitrogen at RT immediately after air has been evacuated.

Evacuated gas	**air (stage 1)**			
Material	Temp	Moisture Level	Time to 100 mTorr[a]	Time to 10 mTorr
Cryo-insulation grade perlite	RT	As received	2 min	60 min
	90 °C	As received	4 min	610 min

[a] 1 Torr = 133.32 Pa.

Evacuated gas	**nitrogen (stage 2)**			
Material	Temp	Moisture Level	Time to 100 mTorr[a]	Time to 10 mTorr
Cryo-insulation grade perlite	RT	Vacuum dried at RT	42 s	146 s
	90 °C	Vacuum dried at RT	44 s	128 s

4. Conclusion

Large-scale storage vessels use bulk fill insulation at moderate vacuum levels, typically employing materials like perlite and hollow glass microspheres. Understanding the evacuation properties of these materials under different temperature and vacuum pressure conditions is essential for the progress of hydrogen-based energy infrastructure, ensuring safety, thermal performance, and long-term cost reduction and sustainability.

Perlite, renowned for its porous structure and low bulk density, was anticipated to facilitate faster evacuation due to larger pathways for gas molecule escape. Conversely, glass bubbles' greater packing efficiency was expected to hinder gas molecule pathways. The research presented herein demonstrates that conditioning of the material has an impact on this behavior and can even lead to a reversal in relative performance, with dry 3M™ Glass Bubbles K1 having faster rates of nitrogen evacuation.

Several reasons for this reversal of performance can be postulated. Firstly, Perlite's irregular shapes could keep residual moisture from leaving the pores of the particles when evacuated from air at room temperature and at 90 °C as well. An alternate or additional mechanism at play could be the relatively fragile nature of the perlite lamellar structure, once expanded, may partially collapse under its own weight or due to thermal cycling stresses; either of which could lead to reduced pathways for gas escape or even gas molecule and moisture entrapment.

The relative evacuation characteristics highlighted herein prompt the reevaluation of the conventional understanding of gas evacuation in bulk-filled insulated cryogenic storage systems. As discussed in the Introduction, preventing hydrogen loss due to boil-off has significant benefits when viewed in the context of societal energy use. With the greater thermal efficiency of 3M™ Glass Bubbles K1 over cryo-insulation grade perlite, there is incentive to further investigate the kinetics and physical processes at play with these bulk-fill insulation materials. Further studies in our lab are underway in which we are exploring the role of different interstitial gases and drying process on the creation of vacuum conditions in perlite and glass bubble insulated vessels.

CRediT authorship contribution statement

Clara Mata: Writing – review & editing, Writing – original draft, Methodology, Investigation, Formal analysis, Data curation, Conceptualization. Rob Hunter: Writing – review & editing, Writing – original draft, Methodology, Investigation, Formal analysis, Conceptualization. Andrew Peterson: Writing – review & editing, Writing – original draft, Methodology, Investigation, Conceptualization. Matt Mortensen: Writing – review & editing, Writing – original draft, Methodology, Investigation, Formal analysis, Conceptualization.

Declaration of competing interest

The authors declare the following financial interests/ personal relationships which may be considered as potential competing interests: The authors are employed by 3M Company, which manufactures and sells glass bubbles.

Acknowledgment

The authors would like to acknowledge Alan Kiraly at Supreme Perlite for providing the generous sample of packaged cryogenic grade perlite. Special thanks are extended to Adam Swanger at NASA Kennedy Space Center for his valuable insights and recommendations during the development of our boil-off analysis.

References

[1] Kim J, et al. Technical feasibility of large-scale transportable liquid hydrogen. Int J Hydrogen Energy 2024;66:499–511.
[2] Kim C, et al. Review of hydrogen infrastructure: the current status and roll-out strategy. Int J Hydrogen Energy 2023;48:1701–16.
[3] Boretti A. Production of hydrogen for export from wind and solar energy, natural gas, and coal in Australia. Int J Hydrogen Energy 2020;45(7):3899–904.
[4] Lee H, et al. Comparative economic and environmental analysis of hydrogen supply chains in South Korea: Imported liquid hydrogen, ammonia, and domestic blue hydrogen. International Journal of Hydrogen economy 2024;78:1224–39.
[5] Makepeace RW, et al. Techno-economic analysis of green hydrogen export. International Journal of Hydrogen Economy 2024;56:1183–92.
[6] Chien FS, et al. Dynamic planning, conversion, and management strategy of different renewable energy sources: a Sustainable Solution for Severe EnergyCrisesin Emerging Economies. International Journal of Hydrogen Economy 2024;46(11):7745–58.
[7] Kim J, et al. Technical feasibility of large-scale transportable liquid hydrogen export terminal. International Journal of Hydrogen Economy 2024;66:499–511.
[8] Munyentwali A, Tan KC, He T. Advancements in the development of liquid organic hydrogen carrier systems and their applications in the hydrogen economy. Prog Nat Sci: Mater Int 2024;34(5):825–39.
[9] Al Ghafri SZS, et al. Hydrogen liquefaction: a review of the fundamental physics, engineering practice and future opportunities. Energy Environ Sci 2022;15:2690–731.
[10] Yin L, Yang H, Ju Y. Review of the key technologies and future development of insulation structure for liquid hydrogen storage tanks. Int J Hydrogen Energy 2024; 57:1302–15.
[11] Yu Y, et al. Design and optimization of the insulation performance of a 4000 m3 liquid hydrogen spherical tank. Processes 2023;11(6):1778.
[12] Ratnakar RR, Sun Z, Balakotaiah V. Effective thermal conductivity of insulation materials for cryogenics LH2 storage tanks: a review. Int J Hydrogen Energy 2023; 48(21):7770–93.
[13] Zhang Fan, et al. The survey of key technologies in hydrogen energy storage. Int J Hydrogen Energy 2016;41(33):14535–52.
[14] Farazmand M, Saadat Z, Sameti M. Above-ground hydrogen storage: a state-of-theart review. Int J Hydrogen Energy 2024;90:1173–205.
[15] Evro S, Oni BA, Tomomewo OS. Carbon neutrality and hydrogen energy systems. Int J Hydrogen Energy 2024;78:1449–67.
[16] Zhang T, et al. Hydrogen liquefaction and storage: recent progress and perspectives. Renewable and sustainable Energy Reviews 2023;176:113204.

[17] Mehr AS, et al. Recent challenges and development of technical and technoeconomic aspects for hydrogen storage, insights at different scales: a state of art review. Int J Hydrogen Energy 2024;70:786–815.
[18] Lin A, Bagnato G. Revolutionizing energy storage: the Latest Breakthrough in liquid organic hydrogen carriers. Int J Hydrogen Energy 2024;63:315–29.
[19] Mulky L, et al. An overview of hydrogen storage technologies – key challenges and opportunities. Mater Chem Phys 2024;321:129710.
[20] Kumar N, Lee SY, Park SJ. Advancements in hydrogen storage technologies: a comprehensive review of materials, methods, and economic policy. Nano Today 2024;56:102302.
[21] Lowesmith BJ. Safety issues of the liquefaction, storage and transportation of liquid hydrogen: an analysis of incidents and HAZIDS. Int J Hydrogen Energy 2014;39 (35):20516–21.
[22] Liu Shitao, et al. Optimizing large-scale hydrogen storage: a novel hybrid genetic algorithm approach for efficient pipeline network design. Int J Hydrogen Energy 2024;66:430–44.
[23] Spatolisano Elvira, et al. Liquefied hydrogen, ammonia and liquid organic hydrogen carriers for harbour-to-harbour hydrogen transport: a sensitivity study. Int J Hydrogen Energy 2024;80:1424–31.
[24] Abdin Z, et al. Large-scale stationary hydrogen storage via liquid organic hydrogen carriers. iScience 2021;24:102966.
[25] Willige A. 4 ways of storing hydrogen from renewable energy | Spectra. 2022. [26] Ratnakar RR, Gupta N, Zhang K, Van Doorne C, Fesmire J, Dindoruk B, Balakotaiah V. Hydrogen supply chain in large-scale LH2 storage and transportation. Int J Hydrogen Energy 2021;46(47):24149–86.
[27] Yang Miao, et al. A review of hydrogen storage and transport technologies. Clean Energy February 2023;7(1):190–216.
[28] Cui Zhenying. Current status and development of hydrogen storage and transportation technologies. Zhongwai Nengyuan 2024;29(7):31–9.
[29] Cheng Q, et al. Review of common hydrogen storage tanks and current manufacturing methods for aluminum alloy tank liners. International Journal of Lightweight Materials and Manufacture 2024;7(2):269–84.
[30] Osman AI, et al. Advances in hydrogen storage materials: harnessing innovative technology, from machine learning to computational chemistry, for energy storage solutions. Int J Hydrogen Energy 2024;67:1270–94.
[31] Lisowski Edward, et al. Study on thermal insulation of liquefied natural gas cryogenic road tanker. Therm Sci 2019;23(4):1381.
[32] Morales-Ospino R, Celzard A, Fierro V. Strategies to recover and minimize boil-off losses during liquid hydrogen storage. Renewable and sustainable Energy Reviews 2023;182:113360.
[33] Muthukumar P, et al. Review on large-scale hydrogen storage systems for better sustainability. Int J Hydrogen Energy 2023;48(85):33223–59.
[34] Aziz M. Liquid hydrogen: a review on liquefaction, storage, transportation, and safety. Energies 2021;14(18):5917.
[35] On-site and bulk hydrogen storage | Department of Energy.
[36] Babac G, Sisman A, Cimen T. Two-dimensional thermal analysis of liquid hydrogen tank insulation. Int J Hydrogen Energy 2024;34(15):6357–63.
[37] Swanger AM, Fesmire JE, Jacobson J, Butts M, Cihlar S. Vacuum pump-down of the annular insulation space for large field-erected liquid hydrogen storage tanks, advances in cryogenic engineering. IOP Conf. Series: Materials Science and Engineering 2023;1301:012066.
[38] Yatsenko EA, et al. Review on modern ways of insulation of reservoirs for liquid hydrogen storage. Int J Hydrogen Energy 2022;47(97):41–54. 41046.
[39] Fesmire JE, et al. Cost-efficient storage of cryogens. AIP Conf Proc 2008;53B: 1383–94. 985 (Advances in Cryogenic Engineering.
[40] Wang P, Liao B, An Z, Yan K, Zhang J. Measurement and calculation of cryogenic thermal conductivity of HGMs. Int J Heat Mass Tran 2019;129:591–8.
[41] Fesmire J.Research anddevelopment history of glass bubbles bulk-fillthermalinsulation systemsforlarge-scale cryogenic liquid hydrogen storage tanks. NASATechnicalReports Server, 2017, Document ID 20180006604, Report KSC-DAA-TN57204.
[42] Demko JA, Fesmire JE, Shu QS. Cryogenic heat management technology and applications for science and industry. first ed. CRC Press; 2022. Ch.2, p.55.
[43] Fesmire JE, et al. Energy efficient large-scale storage of liquid hydrogen - NASA technical reports server (NTRS). 2021.
[44] Swanger A. World's largest liquid hydrogen tank nearing completion. Cryogenic Society of America 2022;38(2).
[45] Sass JP, et al. Glass bubbles insulation for liquid hydrogen storage tanks, NASA center for aerospace information (CASI). 2010.
[46] Fesmire J, Swanger A. Advanced cryogenic insulation systems. Proceedings of the 25th IIR International Congress of Refrigeration; 2019. p. 1732.
[47] Liquid hydrogen outline, idealhy.
[48] Blesing JE, Pelekani C. Seawater desalination: a sustainable solution to world water shortage. 2016.
[49] Schar S, et al. Optimization of sustainable seawater desalination: modeling renewable energy integration and energy storage concepts. Energy Convers Manag 2023;293:117447.
[50] Kim J, et al. A comprehensive review of energy consumption of seawater reverse osmosis desalinization plants. Appl Energy 2019;254:113652.
[51] Electricity consumption in U.S. homes varies by region and type of home, Use of energy explained U.S. Energy Information Administration (EIA).

[52] Gonzalez Monserrate S. The staggering ecological impacts of computation and the cloud. The MIT Press Reader; 2023.
[53] Zhou X, et al. Energy, economic and environmental analysis of a combined cooling, power generation, and energy storage system: a case study of data center in Shenzhen. J Energy Storage 2024;97(Part B):112968.
[54] National Institute of Environmental Health Sciences: Human health impacts of climate change.
[55] Fast facts on climate change and health.
[56] Liu Hengyi. Deaths attributable to anomalous temperature: a generalizable metric for the health impact of global warming. Environ Int 2022;169:107520.
[57] Kim, K. et al., Optimization of proceduresfrom charge ofsilica microsphere to vacuum formation for insulation system of liquefied hydrogen storage tanks, Proceedings of the thirty-third (2023) international ocean and polar engineering conference.
[58] A simple explanation of shear cell powder measurements, Centre for Industrial Rheology.
[59] Brika SE, et al. Influence of particle morphology and size distribution on the powder flowability and laser powder bed fusion manufacturability of Ti-6Al-4V alloy. Addit Manuf 2020;31:100929.
[60] Liu W, et al. Decoding powder flowability: machine learning pioneers the analysis of particle-size distribution effects. Powder Technol 2024;435:119407.
[61] FT4 powder rheometer powder flow tester dynamic methodology, Freeman Technology.
[62] Liu L, et al. Determining random packing density and equivalent packing size of superballs via binary mixtures with spheres. Chem Eng Sci 2019;202:270–81.
[63] 3M™ glass bubbles K1 | 3M United States.

This article was previously published in the International Journal of Hydrogen Energy, Vol. 97, January 6, 2025.

3M Advanced Materials Division
3M Center
St. Paul, MN 55144 USA

Phone 1-800-367-8905
Web www.3M.com/glassbubbles